40 Hz Steady-State Responses in Human Auditory Cortex Depend on GABAergic Neuronal Inhibition

Alessandro Toso[1*], Annika P. Wermuth[1*], Ayelet Arazi[1], Anke Braun[2], Tineke Grent-'t Jong[3,4], Peter J. Uhlhaas[3,4], Tobias H. Donner[1]

[1]Section Computational Cognitive Neuroscience, Department of Neurophysiology and Pathophysiology, University Medical Center Hamburg- Eppendorf, Hamburg, Germany
[2]Department of Psychiatry, Charité Universitätsmedizin, Berlin, Germany
[3]Institute of Neuroscience and Psychology, University of Glasgow, Glasgow, United Kingdom
[4]Department of Child and Adolescent Psychiatry, Charité Universitätsmedizin, Berlin, Germany
* Shared first authorship

Abstract

The 40 Hz auditory steady-state response (ASSR), an oscillatory brain response to periodically modulated auditory stimuli, is a promising, non-invasive physiological biomarker for schizophrenia and related disorders. Because the 40Hz oscillation is injected into the brain by means of the sensory input, ASSR responses measured in the cortex may, in principle, just result from the passive propagation of stimulus oscillations across the auditory pathways, without any intracortical generation or amplification. Alternatively, the ASSR responses may involve cortical circuit interactions that amplify the stimulus-evoked oscillation, which would imply it as mechanistic signature of cortical circuit dysfunctions. Here, we tested whether the 40 Hz ASSR in human auditory cortex depends on two key synaptic components of neuronal interactions within cortical circuits: excitation via N-methyl-aspartate glutamate (NMDA) receptors and inhibition via gamma-amino-butyric acid (GABA) receptors. We combined magnetoencephalography MEG recordings with placebo-controlled, low-dose pharmacological interventions in the same healthy human participants. All participants exhibited a robust 40 Hz ASSR in auditory cortices (stronger on the right) under placebo. The $GABA_A$ receptor-agonist lorazepam increased the amplitude of this ASSR, while no effect was detectable under the NMDA-blocker memantine. Our findings indicate that the 40 Hz ASSR in auditory cortex involves synaptic (and likely intracortical) inhibition via the GABA-A receptor, thus highlighting its utility as a mechanistic signature of cortical circuit dysfunctions involving GABAergic inhibition.

Introduction

An important objective of current translational research is the identification of objective biomarkers of the cortical circuit dysfunctions underlying schizophrenia and other cognitive disorders, such as autism. The auditory steady state response (ASSR), an oscillatory response of the cerebral cortex to a periodically modulated auditory stimulus, has recently gained attention as a candidate neurophysiological biomarker of schizophrenia (1). The ASSR can be measured noninvasively in human patients or healthy participants via electroencephalography (EEG) or magnetoencephalography (MEG) (2, 3). The largest ASSR occurs at stimulus frequencies around 40 Hz (4, 5), pointing to a resonance property of the stimulus-driven neural circuits. A substantial body of evidence indicates a reduction of the ASSR in patients diagnosed with schizophrenia (SCZ) (2, 6-8) as well as in individuals at risk of developing the disorder (8, 9) and first-degree relatives of schizophrenia patients (10, 11). A reduction of the 40 Hz ASSR has also been reported in bipolar disorder (12) and autism (13).

Developing a mechanistic understanding of the 40 Hz ASSR requires delineating the mechanisms generating the ASSR at the level of neural circuits and synapses. As a response to an oscillatory input injected in to the brain, the ASSR may, in principle, simply result from the linear superposition of a sequence of auditory evoked potentials that are faithfully propagated from the inner ear to auditory cortex (4, 14-16). However, some evidence indicates that cortical circuits may amplify ASSRs specifically around the 40 Hz range through intrinsic, recurrent interactions (5, 17). Stimulus-induced gamma band (40-80 Hz) oscillations result from the reciprocal interaction between excitatory pyramidal cells and inhibitory cells (18, 19), with an important role of gamma-amino-butyric acid (GABAergic) inhibitory interneurons (20-22) and glutamatergic N-methyl-aspartate (NMDA) receptor mediated drive of those interneurons from pyramidal neurons (23, 24).

The goal of the current study was to determine whether NMDA and $GABA_A$ receptors are also involved in the generation of 40 Hz ASSRs. To this end, we performed MEG recordings of 40 Hz ASSRs under placebo-controlled pharmacological manipulation of both, $GABA_A$ and NMDA receptors in the same subjects. We found a marked alteration (increase) of ASSRs in auditory cortex under $GABA_A$ receptor stimulation, but not under NMDA receptor blockade.

Material and Methods

Participants

Twenty-three healthy human participants (mean age 28, range 21-40, 9 females) participated in the study after informed consent. The study was approved by the ethics committee of the Hamburg Medical Association. Exclusion criteria are listed in Supplementary Table 1.

Three participants were excluded from the analyses: one due to excessive MEG artifacts and the other two due to not completing all six recording sessions. Thus, we report the results from n = 20 participants (7 females).

Participants were remunerated with 15 Euros for the behavioral training session, 100 Euros for each MEG session, 150 Euros for completing all six sessions, and a variable bonus, the amount of which depended on task performance across all three sessions. The maximum bonus was 150 Euros.

Experimental design

Each participant completed six experimental sessions, each starting with the oral intake of a pill (lorazepam or memantine or placebo), followed by a waiting period of 150 minutes, and the MEG recording session. During MEG, participants were seated on a chair inside a magnetically shielded chamber. Each MEG session was around 2.5 hours in duration and consisted of different tasks including the ASSR task described below. The ASSR task took place usually around 90 min after start of the recording (i.e., 4 h after drug intake).

Pharmacological intervention. We tested for the effects of two different drugs in a double-blind, randomized, placebo-controlled, and crossover experimental design. We used the selective NMDA receptor inhibitor memantine to decrease glutamatergic neurotransmission (25). We used the $GABA_A$ receptor agonist lorazepam to boost GABAergic neurotransmission (26). A mannitol-aerosil mixture was administered as placebo. The dosages were 15 mg for memantine (clinical steady-state dose for adults: 20 mg) and 1 mg for lorazepam (common clinical daily dose between 0.5 and 2 mg). All substances were encapsulated identically to render them visually indistinguishable. Peak plasma concentrations are reached ~3 to 8 hours after administration for memantine (27) and 2 to 3 hours after administration for lorazepam (28). To maximize plasma drug levels during MEG, participants received the pill 150 minutes before the start of recordings. The six sessions were scheduled at least one week apart to allow plasma levels to return to baseline (plasma half-life of memantine: ~60 to 70 hours (27); half-life of lorazepam: ~12.9 hours (28)).

Stimulus and task. During the ASSR task in the MEG we presented 100 repetitions of 1000-Hz carrier tones (duration: 2 s) that were amplitude modulated (ripple tones) at 40 Hz (2). In a subset of sessions, the stimulus was amplitude modulated (AM) at 36.75 Hz (n = 33 over 125 sessions) due to an unpredicted technical change in the experimental setup. Stimuli were presented binaurally through inner ear tubes with an interstimulus interval of on average 2 seconds (jittered between 1.5 and 2.5 s, equal distribution). Ten flat tones (same intensity as ripple tones) were randomly intermixed with the ripple tones. Participants were instructed to fixate a translucent screen (viewing distance: 64 cm) and respond to the flat tones via button press. These trials were not included in the MEG analyses.

Data acquisition

MEG. We used a CTF MEG system with 275 axial gradiometer sensors and recorded at 1200 Hz. Recordings took place in a dimly lit magnetically shielded room. We concurrently collected eye-position data with a SR-Research EyeLink 1000 eye-tracker (1000 Hz). We continuously monitored head position by using three fiducial coils. After seating the participant in the MEG chair, we created and stored a template head position. At the beginning of each following session and after each block we

guided participants back into this template position. We used Ag/AgCl electrodes to measure ECG and vertical and horizontal EOG.

Magnetic resonance imaging. Structural T1-weighted magnetization prepared gradient-echo images (TR = 2300 ms, TE = 2.98 ms, FoV = 256 mm, 1 mm slice thickness, TI = 1100 ms, 9° flip angle) with $1 \times 1 \times 1$ mm^3 voxel resolution were obtained on a 3 T Siemens Magnetom Trio MRI scanner (Siemens Medical Systems, Erlangen, Germany). Fiducials (nasion, left and right intra-aural point) were marked on the MRI.

Data analysis

MEG data were analyzed with a combination of customized scripts (see associated code, which will be made available upon publication) and the following toolboxes: FieldTrip (29) version 20201009 for MATLAB (2021a; The Math-Works, Inc., Natick, MA) as well as MNE (30) and pymeg for Python (https://github.com/DonnerLab/pymeg) established in previous work from our laboratory (31).

Preprocessing. We used an automated algorithm to label artifacts in the continuous time series recorded in each session. Sensor jumps were detected by convolving each sensor with a filter designed to detect large sudden jumps and subsequently by looking for outliers in the filter response. Muscle and environmental artefacts (e.g., cars passing by the vicinity of the MEG room) were detected by filtering each channel in the 100–140 Hz or <1 Hz range, and by detecting outliers that occurred simultaneously in many channels. After removing epochs containing head movements, squid jumps and muscle artifacts, the remaining time-series were then subjected to temporal independent component analysis (infomax algorithm), and components containing blink or heartbeat artifacts were identified manually and removed. We applied a notch filter to remove 50 Hz power line noise and its harmonic (100-150 Hz). The resulting data were segmented in trial epochs of 3 s duration (0.5 s baseline) time-locked to sound onset and all epochs that contained artifacts as defined above were discarded. Finally, the preprocessed data were down sampled to a sampling rate of 400 Hz. For subsequent sensor level analyses, the MEG data were first submitted to a planar-gradient transformation (32).

Spectral analysis. The preprocessed data from each sensor were then submitted to spectral analysis using sliding-window Fourier transform (Welch's method, Hanning tapered, padding: 4 seconds) with a frequency resolution of 0.25 Hz, window length of 500 ms, and step size of 25 ms. For sensor-level analyses, spectral power was then computed, for each time and frequency bin, by taking the absolute value of the (complex-valued) Fourier coefficients and squaring. The ASSR was evaluated by normalizing the power at each time and frequency bin (for topographies and cortical maps: time-averaged power at the stimulus frequency +/- 1Hz) with the power in the pre-stimulus baseline interval (averaged across the range -250 to 0 ms). The stimulus-phase-locked component of the ASSR was evaluated by first averaging the broadband MEG signal across trials in the time domain, followed by spectral analysis and baseline normalization as described above (19).

Source reconstruction. We used linearly constrained minimum variance (LCMV) beamforming (33) to project the MEG data into the space of the underlying cortical sources. To this end, we constructed individual three-layer head models from each individual subject's structural MRI scans. These head models were aligned to the MEG data by a transformation matrix that aligned the average fiducial coil position in the MEG data and the corresponding locations in each head model. Transformation matrices were generated. We computed one transformation matrix per recording session. We then reconstructed individual cortical surfaces from the structural MRIs and aligned the Glasser atlas (34) to each surface. Based on the head model, we generated a forward model ("leadfields") for the computation of LCMV filters that was confined to the cortical sheet (4096 vertices per hemisphere, recursively subdivided octahedron). To compute the LCMV filter for each vertex, the leadfield matrix for that vertex was combined with the trial-averaged covariance matrix of the (cleaned and epoched) data estimated for the stimulus interval (0 to 2 s from stimulus onset). We chose the source orientation with maximum output source power at each cortical location. We projected the broadband time-series into source space, and then extracted power (taking absolute value and squaring) for each frequency and time bin. The power values were extracted at each vertex and finally averaged across all vertices within a given region of interest (see next section).

Regions of interest (ROIs). We used an established anatomical parcellation of the human cortical surface to define ROIs for further analyses (34). For computing cortex-wide maps of the ASSR, the baseline-normalized power response at the stimulus frequency (+/- 1Hz) for the interval from 0.1 to 2 s from stimulus onset was estimated for all 360 parcels of the above atlas. All other analyses collapsed across, the bilateral "early auditory cortex" group, which consists of the following five areas per hemisphere (34): A1, Lateral Belt (LBelt), Medial Belt (MBelt), Para-Belt (PBelt) and retro-insular cortex (RI)). We focused our analyses on this area group as our primary, a priori ROI. We refer to this collapsed ROI as "early auditory cortex" in the following. We used the bilateral central dorsolateral prefrontal cortex group (dlPFC; comprising areas: 9-46d, 46, a9-46v, and p9-46v) as control for anatomical specificity.

Statistical analyses

Sensors showing a significant ASSR were determined using cluster-based permutation tests (a = 0.05, two-sided, n = 10000) across all 40 Hz sessions under placebo condition, with baseline (-250 to 0 ms) and stimulus-induced (100 to 2000 ms) ASSR power averaged across 39-41 Hz as paired samples. Main effects of stimulation at source-level were determined from source reconstructed ASSR power modulations (expressed in percentage relative to pre-stimulus baseline power) at stimulus frequency +/- 1Hz from all 360 Glasser atlas ROIs, using permutation test (two-sided, false discovery rate [FDR]-corrected) across all 20 subjects and sessions under placebo condition.

Source-level ASSRs from early auditory cortex (both total and phase-locked power) were also subjected to cluster-based permutation tests (a = 0.05, two-sided, n = 10000) to find main drug differences i) between 0-2250 ms and stimulus frequency +/- 5 Hz (Figure 3A) and ii) between 0-2250

ms averaged across stimulus frequency +/- 1 Hz (Figure 3B). Permutation tests were used to evaluate drug differences in ASSRs power for the transient component (100-400 ms form stimulus onset and at. stimulus frequency +/- 1 Hz) t and the sustained component (650-1750 ms from stimulus onset and at stimulus frequency +/- 1 Hz) (Figure 3C).

Results

20 healthy participants completed several MEG sessions under either memantine or lorazepam or a glucose placebo (Fig. 1A; see Methods). Memantine is a selective NMDA receptor antagonist (25) and lorazepam is a $GABA_A$ receptor agonist (26), respectively. All substances were administered orally, in a double-blind, randomized, and crossover design. The ASSR stimuli consisted of 1000-Hz carrier tones (duration: 2 s) that were amplitude modulated at either 40 Hz or 36.75 Hz and presented binaurally (Figure 1B) (9).

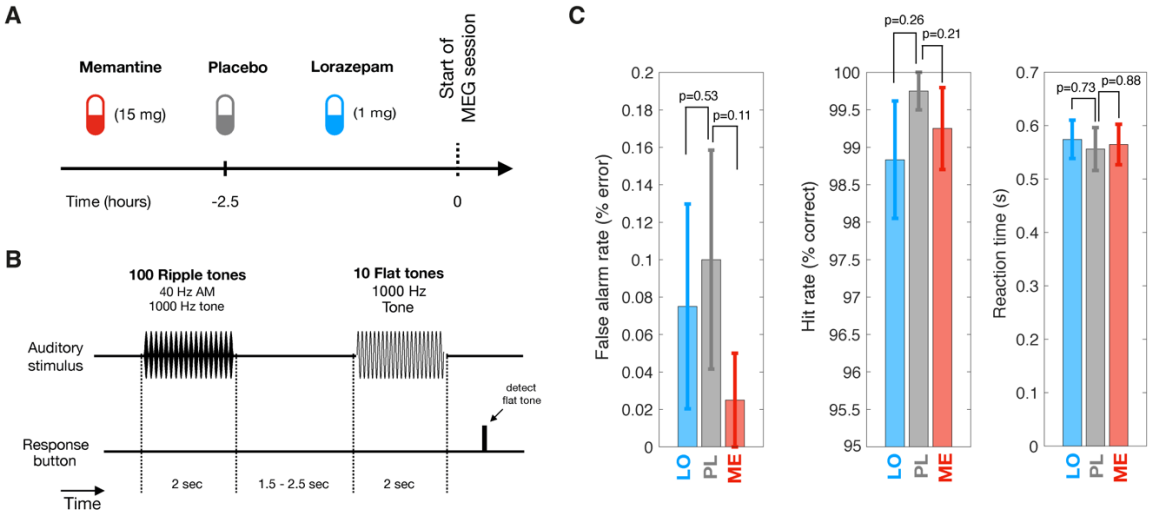

Figure 1. Pharmacological manipulation and task paradigm. (A) Subjects received either Placebo, Lorazepam (1 mg) or Memantine (15 mg) 150 minutes before the start of the MEG session. (B) Task paradigm. (C) Behavioral performance for different drug conditions. Error bars represent SEM. P-values obtained from two-sided permutation tests (N=1000 repetitions) of differences between drug and placebo conditions.

Participants were instructed to fixate a translucent screen and to detect and respond to flat tones (ten in total) that occurred at random times in between the ripple tones with equal intensity levels over time via button press. The flat tones were presented to control attention, but were not used for analyses of the MEG data. The drugs did not affect behavior in this task (Figure 1C), rendering differences in effort or general alertness unlikely causes of any effects on cortical responses described below.

Spatially- and frequency-specific ASSRs

The amplitude-modulated tones produced a robust and specific ASSR during placebo (Figure 2). This response was evident in sensors overlying left and right temporal cortex, with a sustained and significant ($p < 0.01$, cluster-based permutation test) increase in 40 Hz power relative to pre-stimulus interval over

198 right and left frontal-temporal sensors (Figure 2A). The ASSR was also evident in source reconstructions centered on bilateral auditory cortices (stronger in the right hemisphere; Supplementary Figure 1A-B) but spreading to several further temporal, and more distant cortical areas (Figure 2B). All our further analyses focused on bilateral early auditory cortex because this is the first stage of auditory cortical processing and it should (as expected), the most prominent ASSRs. The ASSRs detected in neighboring areas may, at least in part, be due leakage from the auditor cortex ASSR through the spatial filters used for source reconstruction (Materials and Methods).

When we varied the frequency of the stimulus amplitude-modulation (henceforth "stimulus frequency" for brevity) between 40 Hz and 36.75 Hz, the auditory cortex ASSR was strong in both conditions, with a peak frequency that shifted correspondingly in a dependable manner (Figure 2C, see supplementary figure 1 C-D for single subject resolution). By contrast, there was no detectable response in other control regions such as the dorsolateral prefrontal cortex (Figure 2D). When isolating the phase-locked component of the stimulus response (Methods and (19), we found a similarly sustained and frequency-specific, phase-locked component in the early auditory cortex (Figure 2E). Robust ASSRs were detected within each subject (Figure 2F).

In sum, our stimulus protocol and data analysis approach yielded robust, sustained, and lawful ASSRs in early auditory cortex, with a clear phase-locked component. We next quantified the differences in this ASSR between drug and placebo conditions to assess the involvement of glutamatergic and GABAergic synapses in its generation.

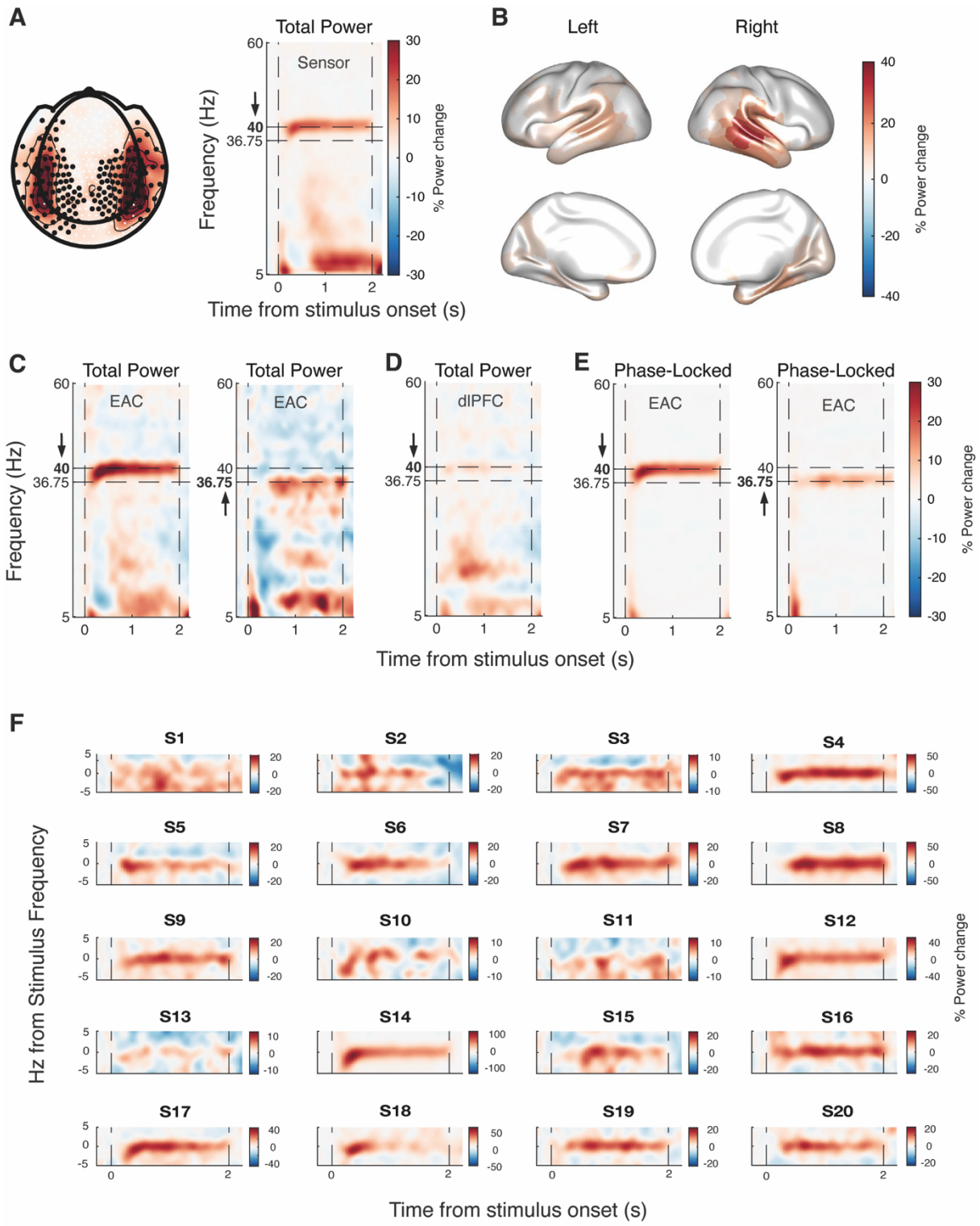

Figure 2. Main effects of ASSR stimulation under placebo condition. **(A)** Left panel depicts % power change relative to pre-stimulus interval at sensor-level averaged across 39 to 41 Hz and 100 to 2000 ms after stimulus onset. Significantly entrained sensors ($p < 0.01$) are marked with black dots; Right panel shows time-frequency representation of average power change relative to pre-stimulus interval for significantly entrained sensors. **(B)** Significant increases of 40-Hz power across 360 Glasser atlas ROIs. **(C)** Time-frequency representation of power changes relative to pre-stimulus interval in 40 Hz sessions (left panel) and 36.75 Hz sessions (right panel) in early auditory cortex. **(D)** Same as panel C but for dlPFC. (E) Time-frequency representation of phase-locked signal components in 40 Hz sessions (left panel) and 36.75 Hz sessions (right panel) in EAC. **(F)** As panel C, but relative to stimulus frequency and shown separately for each individual (S, subject).

Boosting GABAergic transmission increases the ASSRs in auditory cortex

Lorazepam increased the ASSR in early auditory cortex relative to both, placebo and memantine, with no detectable effect for memantine versus placebo (Figure 3A, B). Both the early transient response component (100 to 400 ms from stimulus onset) as well as the later sustained component (650-1750 ms from stimulus onset) were increased under lorazepam (Figure 3C). Lorazepam induced an increased response compared to placebo and memantine, during both the transient component ($p = 0.015$ vs PL, $p = 0.004$ vs ME) the sustained component ($p = 0.011$ vs PL, $p = 0.009$ vs ME) of the ASSR. By contrast, memantine had no detectable effect on the ASSR compared to placebo. By contrast, we found no statistically significant effect on the phase-locked response component when assessed in isolation (Supplementary Figure 2A-B), with a significant increase in power under lorazepam only in the early transient component of the ASSR (Supplementary Figure 2C).

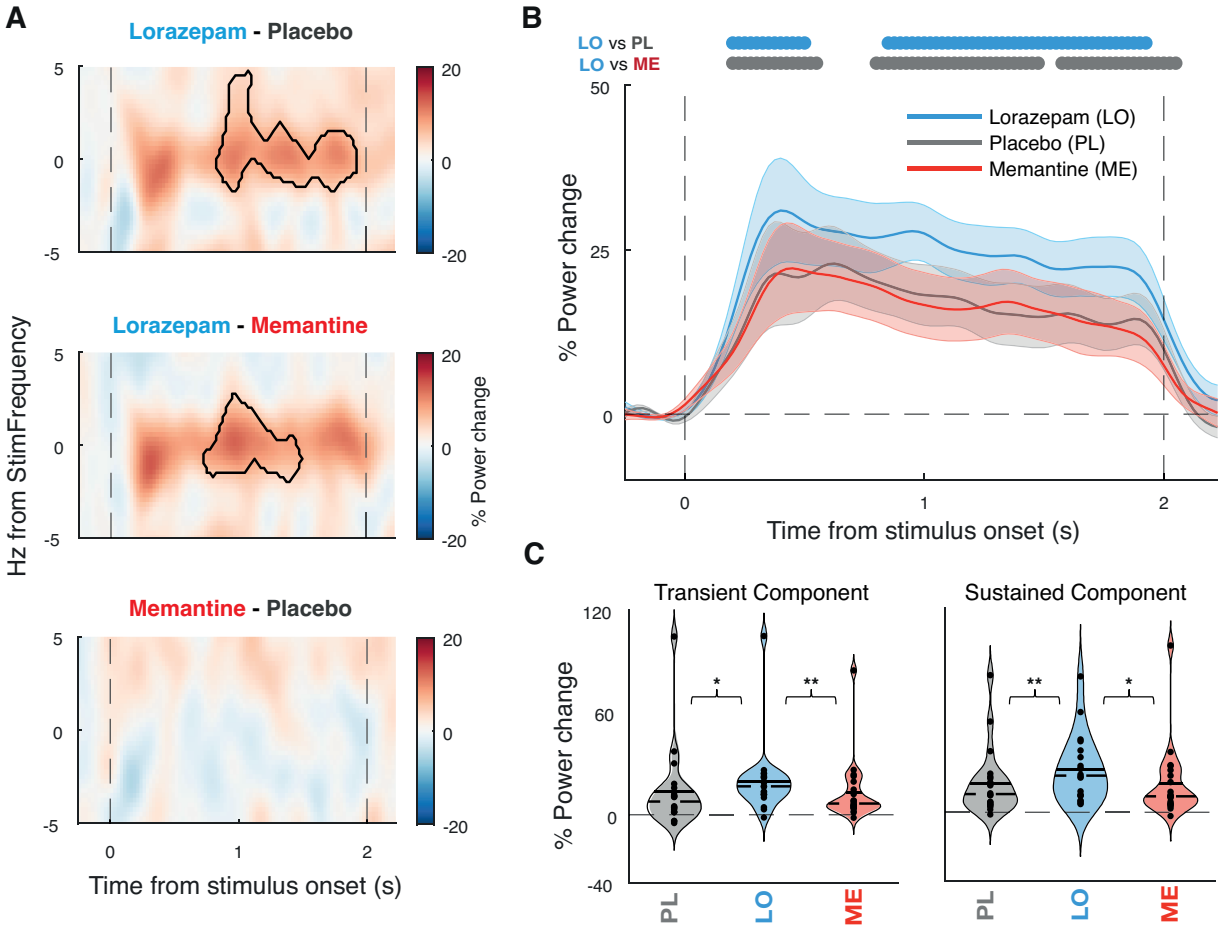

Figure 3. Main drug differences in the auditory steady-state response (ASSR) signals. (A) Time-frequency representation of the power response in early auditory cortex shown as percentage power change between drugs. Contour indicating significant differences between drug conditions ($p < 0.05$; cluster-based permutation test). Dashed vertical lines indicate stimulus onset and offset. (B) Percentage of power change from baseline over time averaged across +/- 1 Hz from stimulus frequency for each drug. Horizontal bars, condition differences ($p < 0.05$; cluster-based permutation test) and shaded error bars representing SEM. (C) % Power change for each drug averaged across stimulus frequency +/- 1 Hz and early (100 to 400 ms, left panel) and late (650 to 1750 ms, right panel) stimulus presentation epochs. Solid line representing the mean and dashed line representing median. Significance estimated via permutation dependent-sample test indicated by stars (* $p < 0.05$, ** $p < 0.01$).

Discussion

To illuminate the synaptic and circuit mechanisms underlying the generation of 40 Hz ASSRs, we performed MEG recordings of ASSRs under placebo-controlled manipulation of both $GABA_A$ and NMDA receptors in human participants. We found that boosting GABAergic transmission through lorazepam robustly increased the 40 Hz ASSR amplitude in auditory cortex, relative to both, a placebo and the NMDA receptor antagonist memantine. Our findings are consistent with previous animal work applying other GABAergic drugs and recordings in hippocampus (35, 36) or temporal cortex (37) and establish an important role of GABA transmission in the 40 Hz ASSR generation in human auditory cortex.

Stimulus-evoked, phase-locked responses and response amplification (i.e., resonance) through intrinsic cortical circuit interactions are likely to differentially shape the transient and sustained response components (19), with early transient response components reflecting predominantly the former and late sustained components reflecting intrinsic circuitry (8, 17, 38). We found that the lorazepam effect was evident in the total response, but not significant in the phase-locked response component only. This is in line with a role of (GABAergic) cortical circuit interactions in the intrinsic amplification of the ASSR within early auditory cortex. Such recurrent cortical synaptic interactions may introduce small phase jitter that leads to cancellation when averaging across trials in order to isolate the phase-locked component (19).

Previous work has shown that the impact of NMDA-R blockade on 40 Hz ASSRs may vary dependent on the type of blocker, drug dose, or the mode of drug administration. Subcutaneous administration of the NMDA-R antagonist ketamine in rodents resulted in an increase of ASSRs power (36, 40). Another rodent study using acute intravenous ketamine infusion yielded, likewise, an ASSR amplitude increase at low dosage, but an amplitude decrease at higher dosage (39), indicating a non-linear dose-response relationship. Ketamine infusion in humans also yielded an ASSR amplitude (41). NMDA blockade via MK-801in anesthetized rats (42) or its injections confined to the thalamus (43), both decreased the ASSR amplitude, while another study reported an increase in ASSR power when MK-801 was administered intraperitoneally in awake rats (44). One human EEG study administering memantine found an ASSR increase at frontal electrodes at 20 mg dosage, but no effect at 10 mg (45). The lack of a detectable memantine effect on the 40 Hz ASSR in auditory cortex in our current study may, therefore, be due to the small, subclinical dosage (15 mg) used here. Future human work should test for the effects of parametric variations of memantine dosage.

Optogenetic manipulations of different interneuron types in animals have established the importance of intracortical inhibition via PV+ interneurons (18, 46) (22) as well as SOM+ interneurons (21) in the intrinsic generation of gamma-band oscillations. 40 Hz ASSRs differ from such intrinsically generated gamma-band oscillations in being driven by a temporal modulated stimulus. Yet, it is conceivable, and consistent with our findings, that the inhibitory cortical circuit motifs for the intrinsic

generation of gamma-band oscillations are also involved in the resonance in response to an external 40 Hz stimulus. It is however noteworthy that drive of PV+ cortically-projecting interneurons of the basal forebrain can also induce a cortical ASSR (47, 48), indicating that a GABAergic manipulation may also alter the ASSR via subcortical pathways.

How does a boost of GABAergic synaptic inhibition increase the amplitude of 40 Hz ASSRs in auditory cortex? Neural circuit modeling has highlighted the importance of the decay time and amplitude of inhibitory postsynaptic currents (IPSC) on PV+ interneurons for the generation of 40 Hz ASSRs (49). Other modeling indicates a possible key role of basket cells among PV+ interneurons subtypes in modulating the amplitude of the response, likely due to their larger number and their different axonal targets compared to chandelier cells (50). Benzodiazepines such as lorazepam increase both IPSC amplitude and decay time (51, 52). In the above neural circuit models, those two increases would produce opposing effects on ASSR power. The increase in ASSR under lorazepam observed in our data is consistent with the IPSC amplitude increase, providing new empirical constraints for circuit models of ASSR generation.

There is substantial evidence for the impairment of cortical inhibition in schizophrenia. Postmortem studies have been shown that schizophrenic patients have a reduction in the GABA transporter GAT-1 (53, 54) and a reduction of GAD-67 (54, 55), an enzyme responsible of GABA synthesis. This down-regulation of inhibitory neurons may be secondary to a deficit in the excitatory drive from pyramidal cells to cortical interneurons (56). Interestingly, mice lacking NMDA-R in PV+ cells showed an impairment in the induction of gamma oscillations by optogenetic activation of cortical interneurons, linking NMDA-R hypofunction to inhibitory down-regulation and gamma oscillations (24). Attenuations in the ASSR found in schizophrenic patients (3, 6-8) and at-risk populations (8, 9) may therefore reflect a either primary or secondary deficit in the inhibitory activity of cortical interneurons. Schizophrenia is associated with aberrant, intrinsically generated, cortical gamma-band oscillations (57, 58) and has been explained in terms of an imbalance between cortical excitation and inhibition (1). Both, intrinsic gamma-band oscillations and cortical excitation-inhibition balance depend critically on intracortical, glutamatergic and GABAergic transmission. Our finding of a GABAergic transmission dependence of the ASSRs is consistent with these previous ideas.

In conclusion, our results indicate that synaptic inhibition via the GABA-A receptor plays a key role in the generation of the 40 Hz ASSR in human auditory cortex. Given the established importance of GABAergic inhibition in schizophrenia and other neuropsychiatric disorders, our findings support the utility of 40 Hz ASSR as a non-invasive signature of aberrations of microcircuit-level processes in human cortex.

Acknowledgments

We thank Karin Reimann for help with subject recruitment, Marlene Petersson, Barbora Schwarzova and Christiane Reissmann for help with data collection, and Christoph Metzner for discussion.

Author contributions

T.H.D, P.J.U , T.G.J, A.T. and A.B. conceptualized the study. A.T., A.W. and A.A. collected the data. A.T., and A.W. analyzed the data. A.T., A.W., T.H.D., P.J.U., and T.G.J, interpreted the results. A.T., A.W., and T.H.D. wrote the first draft of the manuscript. All authors commented on, and edited, the manuscript.

Funding

This work was funded by the German Federal Ministry of Education and Research (BMBF, project numbers 01EW2007B and 01EW2007A) as part of the ERA-NET NEURON consortium *IMBALANCE* (THD and PJU) and Federal State of Hamburg consortium LFF-FV76 (THD).

Competing Interests

The authors declare no competing interests.

References

1. Foss-Feig JH, Adkinson BD, Ji JL, et al.: Searching for Cross-Diagnostic Convergence: Neural Mechanisms Governing Excitation and Inhibition Balance in Schizophrenia and Autism Spectrum Disorders. Biological Psychiatry 81:848-61, 2017
2. Tan HR, Gross J, Uhlhaas PJ: MEG-measured auditory steady-state oscillations show high test-retest reliability: A sensor and source-space analysis. Neuroimage 122:417-26, 2015
3. Thune H, Recasens M, Uhlhaas PJ: The 40-Hz Auditory Steady-State Response in Patients With Schizophrenia: A Meta-analysis. JAMA Psychiatry 73:1145-53, 2016
4. Galambos R, Makeig S, Talmachoff PJ: A 40-Hz auditory potential recorded from the human scalp. Proc Natl Acad Sci U S A 78:2643-7, 1981
5. Pastor MA, Artieda J, Arbizu J, et al.: Activation of human cerebral and cerebellar cortex by auditory stimulation at 40 Hz. J Neurosci 22:10501-6, 2002
6. Kwon JS, O'Donnell BF, Wallenstein GV, et al.: Gamma frequency-range abnormalities to auditory stimulation in schizophrenia. Arch Gen Psychiatry 56:1001-5, 1999
7. Onitsuka T, Tsuchimoto R, Oribe N, et al.: Neuronal imbalance of excitation and inhibition in schizophrenia: a scoping review of gamma-band ASSR findings. Psychiatry Clin Neurosci 76:610-9, 2022

8. Tada M, Kirihara K, Ishishita Y, et al.: Global and Parallel Cortical Processing Based on Auditory Gamma Oscillatory Responses in Humans. Cereb Cortex 31:4518-32, 2021
9. Grent-'t-Jong T, Gajwani R, Gross J, et al.: 40-Hz Auditory Steady-State Responses Characterize Circuit Dysfunctions and Predict Clinical Outcomes in Clinical High-Risk for Psychosis Participants: A Magnetoencephalography Study. Biol Psychiatry 90:419-29, 2021
10. Rass O, Forsyth JK, Krishnan GP, et al.: Auditory steady state response in the schizophrenia, first-degree relatives, and schizotypal personality disorder. Schizophr Res 136:143-9, 2012
11. Hong LE, Summerfelt A, McMahon R, et al.: Evoked gamma band synchronization and the liability for schizophrenia. Schizophr Res 70:293-302, 2004
12. Jefsen OH, Shtyrov Y, Larsen KM, Dietz MJ: The 40-Hz auditory steady-state response in bipolar disorder: A meta-analysis. Clin Neurophysiol 141:53-61, 2022
13. Wilson TW, Rojas DC, Reite ML, et al.: Children and adolescents with autism exhibit reduced MEG steady-state gamma responses. Biol Psychiatry 62:192-7, 2007
14. Presacco A, Bohorquez J, Yavuz E, Ozdamar O: Auditory steady-state responses to 40-Hz click trains: relationship to middle latency, gamma band and beta band responses studied with deconvolution. Clin Neurophysiol 121:1540-50, 2010
15. Bohorquez J, Ozdamar O: Generation of the 40-Hz auditory steady-state response (ASSR) explained using convolution. Clin Neurophysiol 119:2598-607, 2008
16. Ozdamar O, Bohorquez J, Ray SS: P(b)(P(1)) resonance at 40 Hz: effects of high stimulus rate on auditory middle latency responses (MLRs) explored using deconvolution. Clin Neurophysiol 118:1261-73, 2007
17. Ross B, Picton TW, Pantev C: Temporal integration in the human auditory cortex as represented by the development of the steady-state magnetic field. Hearing Res 165:68-84, 2002
18. Buzsaki G, Wang XJ: Mechanisms of gamma oscillations. Annu Rev Neurosci 35:203-25, 2012
19. Donner TH, Siegel M: A framework for local cortical oscillation patterns. Trends Cogn Sci 15:191-9, 2011
20. Cardin JA, Carlen M, Meletis K, et al.: Driving fast-spiking cells induces gamma rhythm and controls sensory responses. Nature 459:663-7, 2009
21. Veit J, Hakim R, Jadi MP, et al.: Cortical gamma band synchronization through somatostatin interneurons. Nat Neurosci 20:951-9, 2017
22. Sohal VS, Zhang F, Yizhar O, Deisseroth K: Parvalbumin neurons and gamma rhythms enhance cortical circuit performance. Nature 459:698-702, 2009
23. Jadi MP, Behrens MM, Sejnowski TJ: Abnormal Gamma Oscillations in N-Methyl-D-Aspartate Receptor Hypofunction Models of Schizophrenia. Biological Psychiatry 79:716-26, 2016
24. Carlen M, Meletis K, Siegle JH, et al.: A critical role for NMDA receptors in parvalbumin interneurons for gamma rhythm induction and behavior. Mol Psychiatry 17:537-48, 2012

25. Johnson JW, Kotermanski SE: Mechanism of action of memantine. Curr Opin Pharmacol 6:61-7, 2006
26. Kienitz R, Kay L, Beuchat I, et al.: Benzodiazepines in the Management of Seizures and Status Epilepticus: A Review of Routes of Delivery, Pharmacokinetics, Efficacy, and Tolerability. CNS Drugs 36:951-75, 2022
27. Noetzli M, Eap CB: Pharmacodynamic, Pharmacokinetic and Pharmacogenetic Aspects of Drugs Used in the Treatment of Alzheimer's Disease. Clinical Pharmacokinetics 52:225-41, 2013
28. Greenblatt DJ, Divoll M, Harmatz JS, Shader RI: Pharmacokinetic Comparison of Sublingual Lorazepam with Intravenous, Intramuscular, and Oral Lorazepam. Journal of Pharmaceutical Sciences 71:248-52, 1982
29. Oostenveld R, Fries P, Maris E, Schoffelen JM: FieldTrip: Open source software for advanced analysis of MEG, EEG, and invasive electrophysiological data. Comput Intell Neurosci 2011:156869, 2011
30. Gramfort A, Luessi M, Larson E, et al.: MEG and EEG data analysis with MNE-Python. Front Neurosci 7:267, 2013
31. Wilming N, Murphy PR, Meyniel F, Donner TH: Large-scale dynamics of perceptual decision information across human cortex. Nat Commun 11:5109, 2020
32. Bastiaansen MC, Knosche TR: Tangential derivative mapping of axial MEG applied to event-related desynchronization research. Clin Neurophysiol 111:1300-5, 2000
33. Van Veen BD, van Drongelen W, Yuchtman M, Suzuki A: Localization of brain electrical activity via linearly constrained minimum variance spatial filtering. IEEE Trans Biomed Eng 44:867-80, 1997
34. Glasser MF, Coalson TS, Robinson EC, et al.: A multi-modal parcellation of human cerebral cortex. Nature 536:171-8, 2016
35. Vohs JL, Chambers RA, Krishnan GP, et al.: GABAergic modulation of the 40 Hz auditory steady-state response in a rat model of schizophrenia. Int J Neuropsychopharmacol 13:487-97, 2010
36. Vohs JL, Chambers RA, O'Donnell BF, et al.: Auditory steady state responses in a schizophrenia rat model probed by excitatory/inhibitory receptor manipulation. Int J Psychophysiol 86:136-42, 2012
37. Yamazaki M, Honda S, Tamaki K, et al.: Effects of (+)-bicuculline, a GABAa receptor antagonist, on auditory steady state response in free-moving rats. PLoS One 15:e0236363, 2020
38. Grent-'t-Jong T, Brickwedde M, Metzner C, Uhlhaas PJ: 40 Hz Auditory Steady State Responses in Schizophrenia: Towards a Mechanistic Biomarker for Circuit Dysfunctions and Early Detection and Diagnosis. Biol Psychiatry, 2023
39. Sivarao DV, Chen P, Senapati A, et al.: 40 Hz Auditory Steady-State Response Is a Pharmacodynamic Biomarker for Cortical NMDA Receptors. Neuropsychopharmacology 41:2232-40, 2016

40. Munch AS, Amat-Foraster M, Agerskov C, et al.: Sub-anesthetic doses of ketamine increase single cell entrainment in the rat auditory cortex during auditory steady-state response. J Psychopharmacol 37:822-35, 2023

41. Plourde G, Baribeau J, Bonhomme V: Ketamine increases the amplitude of the 40-Hz auditory steady-state response in humans. Br J Anaesth 78:524-9, 1997

42. Sivarao DV, Frenkel M, Chen P, et al.: MK-801 disrupts and nicotine augments 40 Hz auditory steady state responses in the auditory cortex of the urethane-anesthetized rat. Neuropharmacology 73:1-9, 2013

43. Wang X, Li Y, Chen J, et al.: Aberrant Auditory Steady-State Response of Awake Mice After Single Application of the NMDA Receptor Antagonist MK-801 Into the Medial Geniculate Body. Int J Neuropsychopharmacol 23:459-68, 2020

44. Sullivan EM, Timi P, Hong LE, O'Donnell P: Effects of NMDA and GABA-A Receptor Antagonism on Auditory Steady-State Synchronization in Awake Behaving Rats. Int J Neuropsychopharmacol 18:pyu118, 2015

45. Light GA, Zhang W, Joshi YB, et al.: Single-Dose Memantine Improves Cortical Oscillatory Response Dynamics in Patients with Schizophrenia. Neuropsychopharmacology 42:2633-9, 2017

46. Bartos M, Vida I, Jonas P: Synaptic mechanisms of synchronized gamma oscillations in inhibitory interneuron networks. Nat Rev Neurosci 8:45-56, 2007

47. Hwang E, Brown RE, Kocsis B, et al.: Optogenetic stimulation of basal forebrain parvalbumin neurons modulates the cortical topography of auditory steady-state responses. Brain Struct Funct 224:1505-18, 2019

48. Kim T, Thankachan S, McKenna JT, et al.: Cortically projecting basal forebrain parvalbumin neurons regulate cortical gamma band oscillations (vol 112, pg 3535, 2015). P Natl Acad Sci USA 112:E2848-E, 2015

49. Vierling-Claassen D, Siekmeier P, Stufflebeam S, Kopell N: Modeling GABA alterations in schizophrenia: a link between impaired inhibition and altered gamma and beta range auditory entrainment. J Neurophysiol 99:2656-71, 2008

50. Metzner C, Zurowski B, Steuber V: The Role of Parvalbumin-positive Interneurons in Auditory Steady-State Response Deficits in Schizophrenia. Sci Rep 9:18525, 2019

51. Kang-Park MH, Wilson WA, Moore SD: Differential actions of diazepam and zolpidem in basolateral and central amygdala nuclei. Neuropharmacology 46:1-9, 2004

52. Pawelzik H, Bannister AP, Deuchars J, et al.: Modulation of bistratified cell IPSPs and basket cell IPSPs by pentobarbitone sodium, diazepam and Zn
:: dual recordings in slices of adult rat hippocampus. Eur J Neurosci 11:3552-64, 1999

53. Konopaske GT, Sweet RA, Wu Q, et al.: Regional specificity of chandelier neuron axon terminal alterations in schizophrenia. Neuroscience 138:189-96, 2006

54. Lewis DA, Hashimoto T, Volk DW: Cortical inhibitory neurons and schizophrenia. Nat Rev Neurosci 6:312-24, 2005

55. Straub RE, Lipska BK, Egan MF, et al.: Allelic variation in GAD1 (GAD67) is associated with schizophrenia and influences cortical function and gene expression. Mol Psychiatry 12:854-69, 2007

56. Chung DW, Fish KN, Lewis DA: Pathological Basis for Deficient Excitatory Drive to Cortical Parvalbumin Interneurons in Schizophrenia. Am J Psychiatry 173:1131-9, 2016

57. Uhlhaas PJ, Singer W: Abnormal neural oscillations and synchrony in schizophrenia. Nat Rev Neurosci 11:100-13, 2010

58. Bianciardi B, Uhlhaas PJ: Do NMDA-R antagonists re-create patterns of spontaneous gamma-band activity in schizophrenia? A systematic review and perspective. Neurosci Biobehav Rev 124:308-23, 2021

Supplementary Material

Supplementary Table 1: Exclusion criteria

History of any neurological or psychiatry disorders.
Hearing disorder.
History of any cardiovascular disease.
History of any liver or kidney disease or metabolic impairment.
History of any chronic respiratory disease (e.g., asthma).
History of hyperthyroidism or hypothyroidism.
Pheochromocytoma (present or in history)
Allergy to medication.
Known hypersensitivity to memantine or lorazepam.
Family history of epilepsy (first or second degree relatives).
Family history of psychiatric disorders (first or second degree relatives).
Established or potential pregnancy.
Claustrophobia.
Implanted medical devices (e.g., pacemaker, insulin pump, aneurysm clip, electrical stimulator for nerves or brain, intra-cardiac lines).
Any non-removable metal accessories on or inside the body.
Having impaired temperature sensation and / or increased sensitivity to heat.
Implants, foreign objects and metal in and around the body that are not MRI compatible
Rejection to receive information about accidental findings in structural MR images
Hemophilia
Frequent and severe headaches, dizziness, or fainting.
Regularly taking medication or have taken medication within the past 2 months.

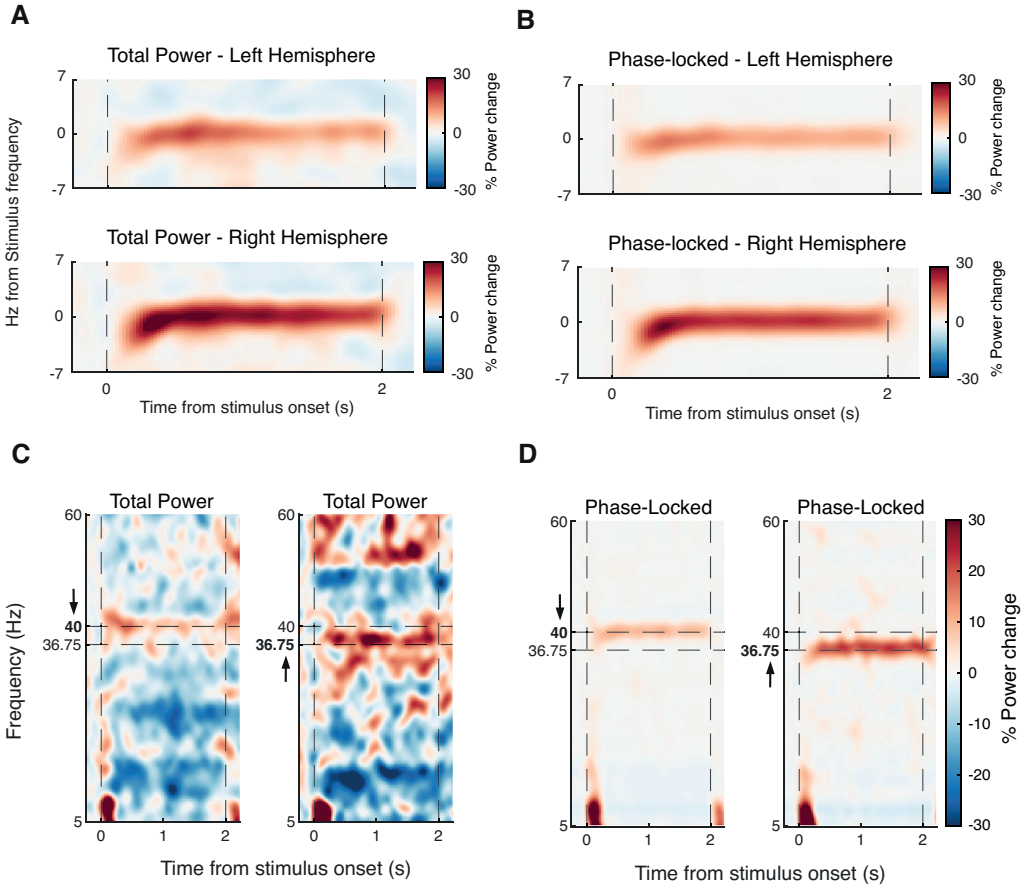

Supplementary Figure 1. Single subject data and hemispheric lateralization. (A) Time-frequency representation of power changes relative to pre-stimulus interval for left (upper panel) and right (lower panel) EAC. (B) Same as (A) but phase-locked signal components. (C) Time-frequency representation of power changes relative to pre-stimulus interval in a 40 Hz session (left panel) and a 36.75 Hz session (right panel) in early auditory cortex for one subject. (D) Time-frequency representation of phase-locked signal components in a 40 Hz session (left panel) and a 36.75 Hz session (right panel) in early auditory cortex for one subject

.

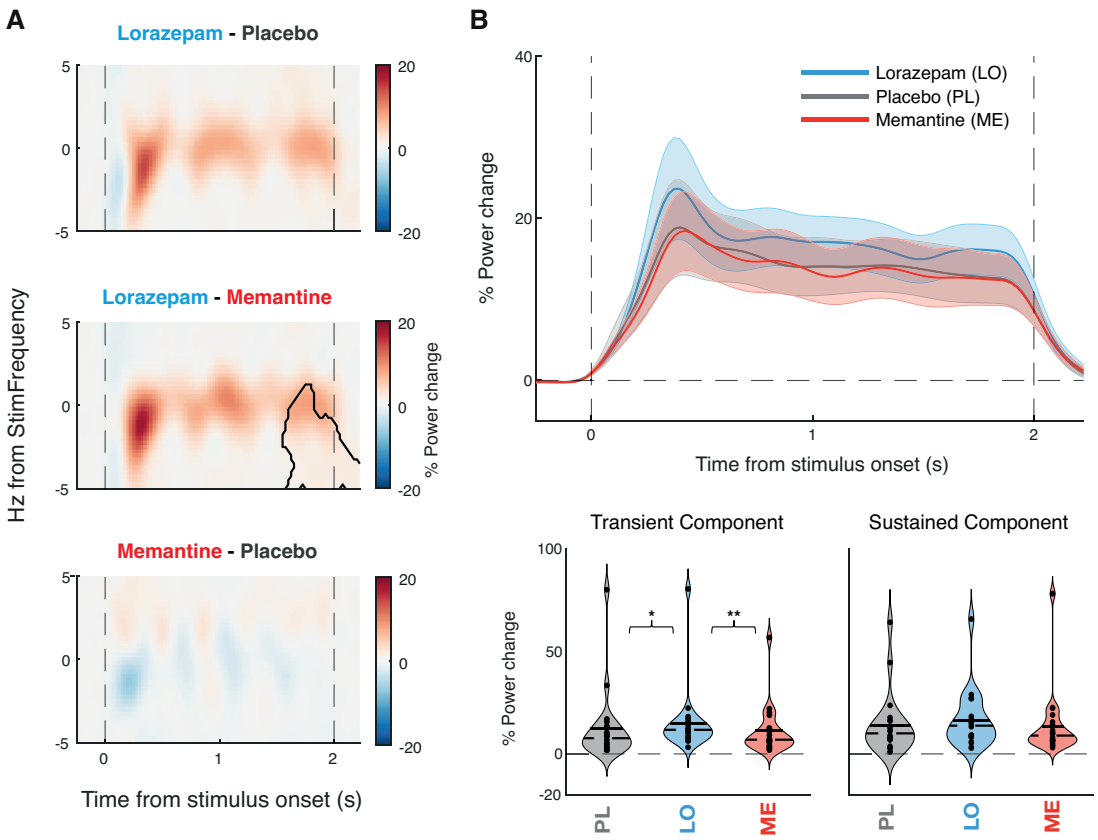

Supplementary Figure 2. Drug effects on phase-locked response component. (A) Time-frequency representation of the power response in Early Auditory cortex shown as percentage power change between drugs. Contour indicating significant differences between drug conditions estimated via Monte Carlo cluster-based permutation dependent-sample t-test. Dashed vertical lines indicate stimulus onset and offset. (B) % Power change over time averaged across stimulus frequency +/- 1 Hz for each drug with dots above indicating significant differences between drugs ($p < 0.05$) and shaded error bars representing SEM. (C) % Power change for each drug averaged across stimulus frequency +/- 1 Hz and early (100 to 400 ms, left panel) and late (650 to 1750 ms, right panel) stimulus presentation epochs. Solid line representing the mean and dashed line representing median. Significance estimated via cluster-based permutation dependent-sample test indicated by stars (* $p < 0.05$, ** $p < 0.01$).